

E. P. Busso, D. Boivin, D. L  v  que
(ONERA)

E-mail : esteban.busso@onera.fr

DOI : 10.12762/2016.AL12-02

On Recent Advances in Microstructural Characterization and *In-Situ* Testing Techniques to Study Material Behavior

The deformation fields within grains in polycrystalline materials are generally highly heterogeneous and can be the precursors to the nucleation of micro-cracks or cavities. Such behavior is conditioned by microstructural features, such as grain structure, texture, morphology, and size. The understanding of the inter-relationship between the material's microstructural characteristics and complex deformation and damage phenomena is crucial to the formulation of structural integrity assessments of engineering components, since they constitute the physical bases of the required constitutive models of deformation and failure.

In this work, an overview is provided of recent experimental techniques developed at ONERA and elsewhere to characterize the microstructure and to measure the deformation of metallic materials. Some of the most promising characterization, measurement and identification techniques and methods used to develop, calibrate and validate physics-inspired constitutive models will be discussed, and illustrative examples will be given. It will be shown that the individual use of traditional interferometric, characterization and testing techniques is being replaced by the combined use of state-of-the-art techniques based on image correlation (2D and 3D), *in-situ* and *ex-situ* scanning electronic microscopy (SEM), EBSD, amongst others. Discussions about future trends, including the great potential offered by the combination of *in-situ* techniques at various scales with real time computations, are presented.

Introduction

The development of new materials and the optimization of existing ones require an understanding of how their microstructures at all relevant scales affect their mechanical and functional properties. Such relationships can be very complex, since they generally involve physico-chemical processes that act during their entire life cycle. In order to reduce development and characterization costs, accurate multi-physics and multi-scale models based on sound physical principles are needed. In addition, suitable characterization, identification and validation methods are required at different microstructural scales. These may involve measurement techniques that need to be coupled with the numerical integration of complex constitutive material models (e.g., see [19]), sometimes in real time. Handling the resulting large amount of data that need to be stored is becoming a major challenge, since the resolution and accuracy of detailed microstructural measurements is continuously increasing. An additional

difficulty is the efficient visualization of the very large amount of data that needs to be handled. For instance, a single 3D image obtained by computed tomography and reconstructed numerically may require up to 16 GBytes of computer disk space [10]. Furthermore, the measurement of full fields by techniques such as image correlation is equally demanding in terms of digital storage capabilities [23]. However, it is the simultaneous use of multiple observation and measurement techniques such as those described above that offers exciting new opportunities for the development and calibration of physics-inspired constitutive models of materials with complex heterogeneous microstructures.

In this work, the challenges associated with some of the most promising characterization, measurement and identification techniques to study the mechanical behavior of materials will be addressed.

However, since this overview is not intended to be exhaustive by any means, special emphasis is placed on 2D and 3D imaging and *in-situ* micromechanical scanning electronic microscopy (SEM) testing techniques, coupled with electron back-scattered diffraction (EBSD), developed at ONERA and elsewhere. Other important experimental techniques, such as transmission electronic microscopy (TEM), energy-dispersive X-ray spectroscopy (EDS), thermography and tomography, should be combined with those to be discussed next, in order to address a broader range of physico-chemical phenomena.

2D and 3D Measurement Methods

The study of material behavior has traditionally relied on either *in-situ* or *ex-situ* surface measurements of deformation fields, as previously discussed, and on post mortem characterizations of the material microstructure. Since the mid 90s, traditional interferometric techniques (e.g., speckle, Moiré, holography) to measure deformation fields have gradually been replaced by a new family of techniques based on image correlation: 2D-Digital Image Correlation (2D-DIC) (*i.e.*, correlations of images of a surface acquired with a single camera) (e.g., [10][13]), and by 3D-DIC (*i.e.*, measurements of 3D surface shapes and displacements using two cameras) (e.g., [12][15]). However, the pertinence of relying on surface information to interpret bulk phenomena is not sufficient in many instances. In the last decade, the ability to visualize the volume of a material in three dimensions (3D) in a non-destructive way at the scale of a few micro-metres or less has opened up exciting new ways to study and characterize the microstructure and behavior of a broad range of materials [28]. An example is the detailed local microstructural information that can be obtained about, for instance, grain morphology, defect population, and damage, using tomography through either an X-ray source of a synchrotron or a laboratory scale micro-tomograph [5]. The data associated with the digitized material volume obtained from such 3D imaging techniques are then combined with suitable algorithms to identify the morphology of the microstructural features of interest and local displacement fields. The resulting techniques are known as either Digital Volume Correlation (DVC) or Volumetric DIC (V-DIC).

In what follows, a discussion of the main methods used for 2D and 3D digital image correlation at ONERA will be presented and compared with current practice. This will include details about efficient algorithms and parallel computing implementation, in particular the fast option offered by Graphic Processing Units (GPUs). Illustrative examples on the use of 2D and 3D-DIC in aeronautical materials and structures in terms of both computational performance and accuracy will be presented and discussed.

Basic principles and approaches

Full-field measurements in solids using imaging tools follow either classical global [11] and local [3] approaches, and the pixel-wise displacement estimate (referred to as "dense" by the authors) approach proposed recently by ONERA [15], which is a particular type of local approach. Their main differences concern the choice of reference domain used. To illustrate that point, let us recall the basic principle on which DIC is based.

DIC relies on a cross-correlation to measure shifts in datasets by finding the maximum of the correlation between pixel intensities on two or more corresponding images. If a vector \mathbf{x} defines the position of a point in the reference image, and $\mathbf{u}(\mathbf{x})$ the displacement vector associated with the new position of that point in the new configuration, then the function that defines the characteristics of the point (e.g., the intensity of the pixel's grey-scale at that point) in the reference image can be expressed as,

$$f(\mathbf{x}) = g(\mathbf{x} + \mathbf{u}(\mathbf{x})) \quad (1)$$

where g is the corresponding gray-scale value in the image's new deformed configuration. The main objective of all image correlation algorithms is to determine the transformation, $\mathbf{u}(\mathbf{x})$, in the region of interest, Ω , of the reference image, knowing the values of f and g . The correlation procedure must be carried out in a certain domain and solved by minimizing a given quantity. The most commonly used minimization quantity is that defined by the least square difference between the gray-scale values of the images over the domain of interest, Ω . Here,

$$\eta = \int_{\Omega} [f(\mathbf{x}) - g(\mathbf{x} + \mathbf{u}(\mathbf{x}))]^2 d\mathbf{x} \quad (2)$$

However, the problem is ill-posed, since the available information, e.g., the gray-scale values of the pixels, is insufficient to compute the displacement vector, $\mathbf{u}(\mathbf{x})$, that is, the number of unknowns is greater than the number of equations. To overcome that problem, the correlation procedure must rely on additional hypotheses associated with the definition of the domain to be correlated.

In classical local approaches, the domain Ω is defined by small correlation windows in the region of interest, each window containing more than one pixel, the number determined by both the spatial resolution desired and the degree of overlapping between windows, if any. This issue will be further discussed below. In contrast, the domain Ω in global approaches is defined by the whole region of interest, rather than just by a small window. The discretization of the global region is generally done following a similar scheme to that of the finite element method. Thus, the displacement fields can be interpolated according to a relation of the form,

$$\mathbf{u}(\mathbf{x}) = \sum_{n \in N} u_n \Psi_n(\mathbf{x}) \quad (3)$$

Here, u_n are the degrees of freedom and Ψ_n are the chosen interpolation vector functions. The solution of the correlation problem in the global approaches requires the minimization of Eqn. 2 assuming the functional form of the displacements given by Eqn. 3. This is done by seeking the optimal values of the unknown displacement coefficients, u_n . However, in local approaches, Eqn. 3 is not required to carry out the correlation itself, but it is instead used as a post-processing tool to smooth the estimated displacement fields.

In order to deal with the main challenges resulting from the manipulation of the huge amount of data obtained through 2D and 3D imaging, fast processing algorithms such as those originally developed for particle image velocimetry (PIV) used in experimental fluid mechanics, have recently been developed for 2D-DIC or 3D-DIC [1]. One such

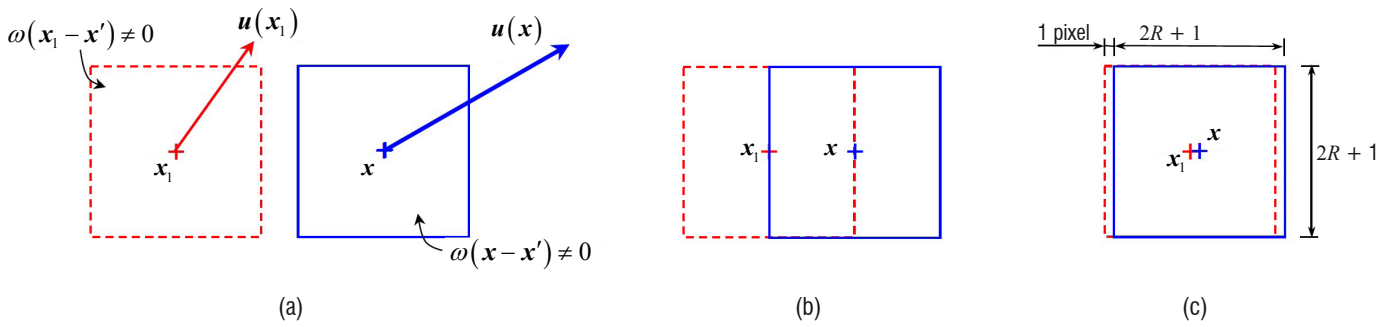


Figure 1 – Illustration of the possible relative configurations between two neighboring correlation windows centered at pixels x and x_1 , for which the displacements $u(x)$ and $u(x_1)$, respectively, are calculated: (a) non-overlapping and (b) partially overlapping window configurations typical of classical local DIC approaches, and the (c) maximum possible overlapping window configuration of the FOLKI-D method. Each local window is delimited by its corresponding weight function, ω

contribution is the recent work by Le Besnerais *et al.* [15], which describes ONERA's fast and promising image correlation method for solid mechanics applications, named FOLKI-D (a French acronym for the Iterative Lucas-Kanade Optical Flow). The FOLKI-D method [14] is an extension of Lucas' and Kanade's original algorithm [16] adapted for PIV in [7].

In contrast to the classical global DIC approach, ONERA's pixel-wise displacement estimate approach (FOLKI-D) [15] is a local one, since it relies on the information associated with a window centered on a particular pixel to calculate its displacement. The minimizing quantity is similar to that given in Eqn. 2, but it is performed over a single window at a time using a weight function $\omega(x - x')$ – with ω typically representing a $(2R + 1)^2$ square shaped window, and R being the desired scaling parameter. Then,

$$\eta_x(\mathbf{u}) = \sum_{x' \in \Omega} \omega(x - x') [f(x') - g(x' + \mathbf{u}(x))]^2 \quad (4)$$

The minimization of Eqn. 4 is then carried out using a Gauss-Newton iterative algorithm.

Most classical local approaches consider correlation windows that either do not overlap at all, or that exhibit small partial overlaps. In contrast, FOLKI-D estimates the displacement of each pixel by considering that neighboring correlation windows exhibit the maximum possible overlap between them. Short of these being 100% coincidental, such configuration implies that the spacing between neighboring windows is just a single pixel. This point is illustrated in Figure 1, which shows the possible relative configurations between two neighboring correlation windows centered at pixels x and x_1 , with (a) representing non-overlapping and (b) representing partially overlapping window configurations, both typical of classical local DIC approaches, and (c) the maximum possible overlapping window configuration of the FOLKI-D method.

It should be pointed out that, even though the minimization of a relation of the type given by Eqn. 2 is performed independently for each pixel, all minimization operations can, in principle, be performed simultaneously on all pixels of the image. However, the use of such an approach on the maximum possible overlapping window configuration illustrated in Figure 1(c) would result in an excessively large number of redundant computations to update each displacement vector independently, since a pixel shares most

of its corresponding window with its neighbors. In order to overcome this problem, the FOLKI-D method relies on a first order Taylor expansion of Eqn. 4 and on the reformulation of the problem in terms of global convolutions and pixel-wide operations. As a result, the optimization only involves regular and local operations over the whole image, leading to a method which is highly efficient and suitable for modern parallel computing architectures, such as GPUs. See [15] for further details.

The pixel-wise displacement estimate DIC approach offers another considerable advantage with respect to the classical global approaches, since there are no a priori assumptions to be made about the nature of the displacement fields, with the corresponding gain in computing efficiency, accuracy and potential for parallelization using, for instance, GPUs. These issues will be discussed later in the text, in one of the case studies (multi-scale deformation behavior of a woven composite).

Another promising application of DIC or DVC is when it is combined with finite element (FE) modeling and remeshing techniques to locate and introduce into the FE model microcracks in either quasi-real time or as a post-processing. Recent work carried out at ONERA [8] has proposed a method whereby the crack growth path can be identified from the image processing by following the peak of a representative local material degradation measure, such as the magnitude of a displacement discontinuity between neighboring pixels.

For additional discussions of current issues and future trends in 2D-DIC, 3D-DIC and DVC, refer to [29].

Representative experimental test cases

In this section, two experimental test cases reported in [15] involving 3D surface displacement field measurements using ONERA's FOLKI-D algorithm are presented.

The first test case consists of a stereographic 3D-DIC measurement during the uniaxial compression of a carbon-epoxy laminate composite panel after an impact test. Such a testing procedure is widely used by the aeronautic industry for certification purposes and to demonstrate repair process worthiness. In this test, two images are recorded at each instant, to compute both the specimen shape and

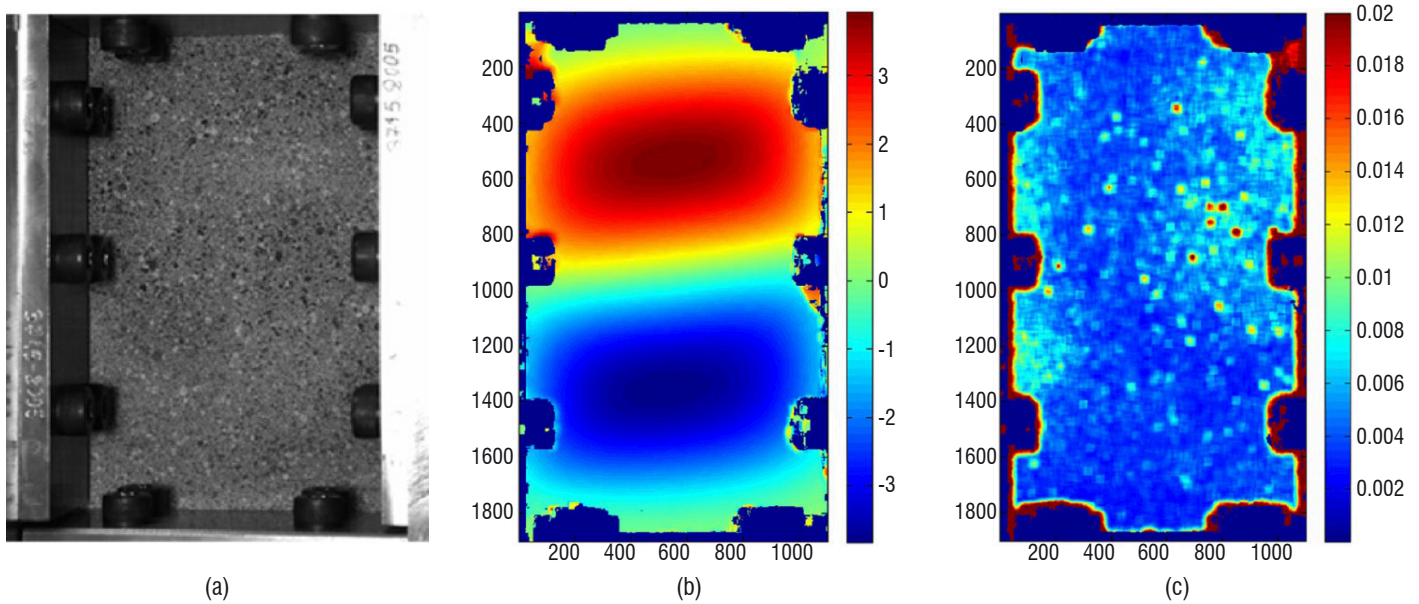


Figure 2 – Uniaxial compression of a carbon-epoxy laminate composite panel after an impact test: (a) specimen, (b) out-of-plane displacement component, and (c) uncertainty estimation obtained with FOLKI-D [15]

the 3D displacement field. Figure 2 shows (a) an image of one of the specimen's sides, (b) a plot of the measured out-of-plane displacement component, and (c) the distribution of the uncertainty estimation obtained with FOLKI-D. The scales in Figures 2(b) and (c) are in pixel units. It can be seen from Figure 2(b) that the measured out-of-plane displacement component distribution implies that specimen buckling has occurred. A comparison between the accuracy of the computed displacements and those obtained using a commercially available code showed that they differed by less than 2.5%. However, the computing time to process the two stereographic 2 MPixel images of FOLKI-D was found to be 24 times faster than the commercial code. Another advantage of FOLKI-D is that it enables information close to the specimen borders to be obtained due to the large number of the resulting displacement vectors (2 million for the window shown

in Figure 2's case, against 32 k vectors for the commercial code). Finally, the uncertainty distribution of the computed displacement at each pixel plotted in Figure 2(c) is obtained from a classical local statistical analysis.

The second test case is intended to illustrate the robustness of FOLKI-D when dealing with degraded image textures, as is usually the case when measurements are conducted in high-temperature environments. Here, the growth of a fatigue crack at 900°C in a polycrystalline superalloy plate with a center hole is investigated. This test is representative of local conditions seen in aero-engine combustion chambers. Figure 3 shows the crack configurations after (a) 47000 and (b) 53000 cycles at the maximum cycle load, and (c) and (d) the vertical displacement component fields measured by FOLKI-D

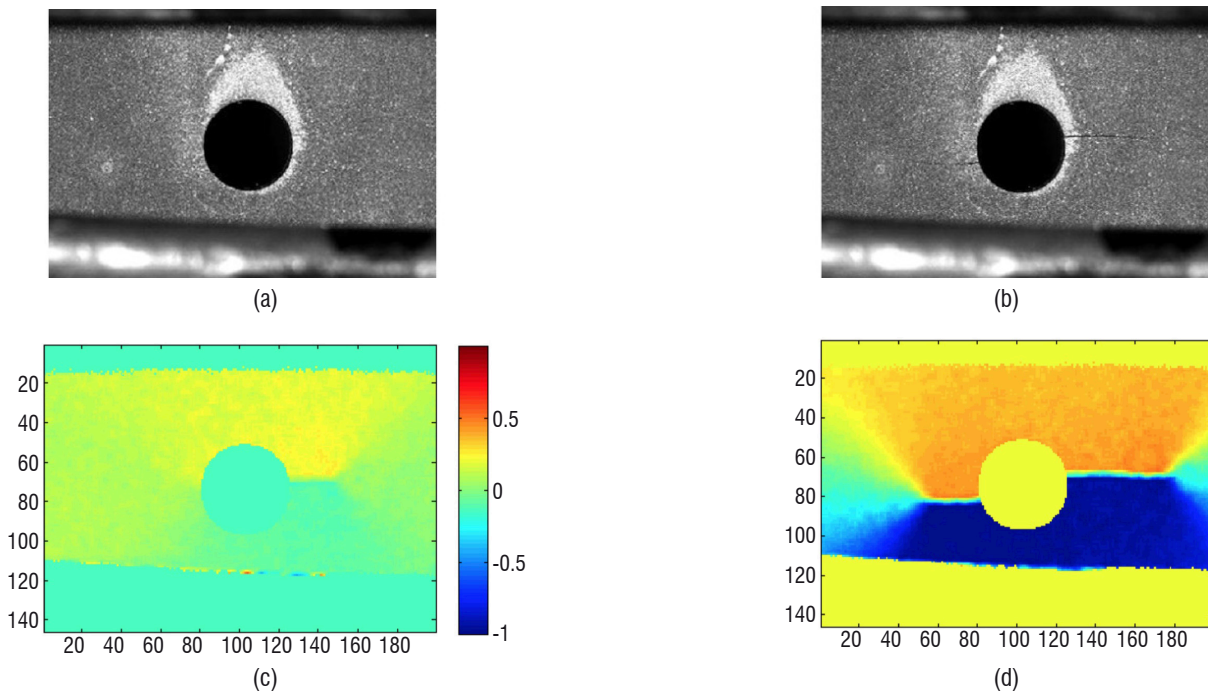


Figure 3 – Growth of a fatigue crack at 900°C in a polycrystalline superalloy plate with a center hole: crack configurations after (a) 47000 and (b) 53000 cycles at the maximum cycle load, and (c) and (d) vertical displacement component fields measured by FOLKI-D corresponding to the configurations in (a) and (b), respectively [15] (the applied load is in the vertical direction)

corresponding to the configurations in (a) and (b), respectively [15]. It should be pointed out that, despite the low contrast on the specimen surface, the FOLKI-D results were capable of providing an accurate estimate of the actual crack lengths and crack tip positions by relying on a local discontinuity criterion. As discussed in [15], high-temperature DIC measurements require that the light emission from the heated surface be minimized by the use of suitable filters [9] and by ensuring that the time between images is sufficiently short to avoid the development of oxidation-related surface texture. Nevertheless, uncertainties in the measured displacements in some regions where the local variance of the calculated residuals is high were found to be up to 0.05 pixel.

Combined Local Microstructural Characterization and Measurement Methods

Scanning electronic microscopes (SEM) are not just sophisticated high-resolution instruments to observe the surface of samples at the sub-micron scale. They can also be used to identify the crystallographic characteristics and chemical composition of the sample when coupled with electron back-scattered diffraction (EBSD) and energy-dispersive X-ray spectroscopy (EDS) or wavelength dispersive spectroscopy (WDS) techniques, respectively.

An analysis by EBSD provides information about the individual grains in the material. A typical inverse pole figure (IPF) produced by EBSD of a typical AISI 316L-type austenitic stainless steel is shown in Figure 4 [17]. Here, Figures 4(a) and (b) are IPFs of the microstructure in the annealed and cold-rolled state, respectively. The close-up image of the microstructure in the cold-rolled state in Figure 4(b) shows also the slip traces within the grains.

The microscope's electronic beam can also be used as a micro-lithography electronic tool to create surface patterns on the sample to be tested and thus serve as a micro-extensometer to measure its deformation during either *in-situ* or *ex-situ* micromechanical tests. This capability to link several observation and characterization techniques has recently opened up a wide range of opportunities to study the behavior of materials with heterogeneous microstructures. The simultaneous acquisition of crystallographic information and deformation fields enables a qualitative and quantitative understanding of the material behavior, and provides local information to validate local constitutive material and life prediction models.

In what follows, two examples are given of recent original work carried out at ONERA based on a multiple material characterization of high-temperature alloys used in aerospace applications.

Combined EBSD and *in-situ* micromechanical SEM testing to measure high-temperature grain boundary sliding in a Ni-base superalloy

Intergranular creep is one of the important mechanisms that conditions the behavior and lifetime of high-temperature gas turbine disc and blades. Generally, the amount of grain boundary (GB) sliding which contributes to the macroscopic time-dependent deformation is quite small, of the order of tens of nanometers, thus specialized microscopy techniques are needed to measure such deformation. One of the common techniques used for that purpose is known as "marking", whereby some visible markers are deposited on the

material surface to serve as a visual reference and thus enable small relative GB displacements to be measured during deformation. The technique developed at ONERA will be discussed later in the text.

A combination of EBSD, which provides information about the local crystallographic deformation, with marking at the grain scale was undertaken at ONERA to study the intergranular GB sliding due to creep in a Ni base superalloy at 850°C. Even though the method is relatively simple, its development requires expertise in processing, heat treatments, *in-situ* micro-extensometry within the chamber of an SEM, analysis by EBSD, and complex data processing.

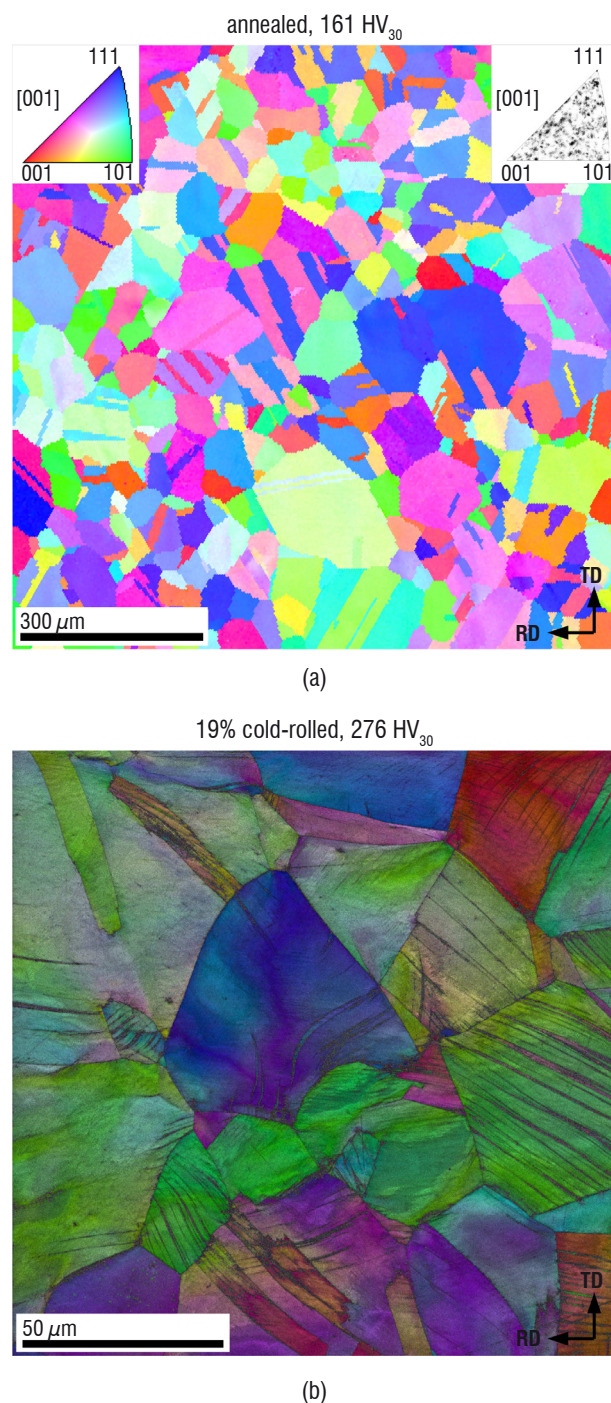


Figure 4 – Microstructure of an austenitic stainless steel observed by EBSD: (a) annealed state shown in inverse pole figure (IPF) and (b) cold-rolled state, in a close-up view, shown by a superposition of the IPF and image quality maps [17]

The results to be reported here are some of those obtained as part of the work by Thibault [31] [32]. Note that the discussion of these representative results is intended to illustrate the potential and accuracy of advanced characterization and *in-situ* testing techniques, and it does not constitute an exhaustive study of superalloy creep behavior. For more detailed and complete studies conducted in this area at ONERA, it is suggested that the reader refers to [25, 26, 27, 31, 32].

Identification and analyses of the grain boundary characteristics by EBSD

In order to study the characteristics of grain boundaries, the coincidence site lattice (CSL) model is used. The model enables the nature of the GBs, such as highly misoriented ones ($\theta \geq 15^\circ$) to be defined. Generally, GBs are classified by their coincidence index, denoted by Σ . For instance, grains that share a $\Sigma 5$ boundary contain $1/5^{\text{th}}$ of atoms located on common lattice sites. Thus, boundaries are said to be generic if $\Sigma > 29$, and special if $\Sigma \leq 29$ [21]. Amongst the special boundaries, it is worth identifying those where the degree of lattice coincident sites is the maximum, namely the $\Sigma 3$ boundaries, often associated with twins and known as twin boundaries. The expectation is that boundary structures with low Σ values will be more regular than a general boundary and hence would have low energies because of their good atomic fit. This consideration is central to the concept of "grain boundary engineering", which relies on maximizing the fraction of CSL boundaries as a way of increasing the material strength.

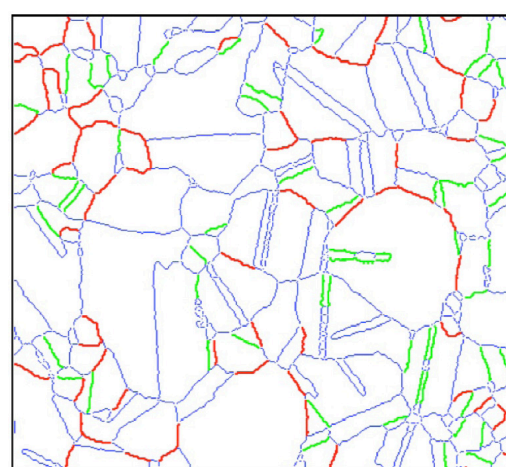
The processing of EBSD information can take many different forms. For instance, it can be used to identify and visualize a particular type of grain boundary, such as the $\Sigma 3$ boundaries and generic ones, as shown in the example of Figure 5. Here, Figure 5(a) shows the GB network extracted from the EBSD information: red GBs are of the $\Sigma 3$ type, green ones are generic ones, both are of between 20 to 40 μm in length, and blue ones are generic GBs of other sizes. Figure 5(b) shows a distribution of the GB lengths identified in Figure 5(a). Other types of information can be inferred from EBSD measurements, depending on the criteria used. For instance, EBSD software enables the identification of individual GB intersections, and the fraction of GB intersections connected to 0, 1, 2 or 3 boundaries of the $\Sigma 3$ type, for instance. In reality, such intersections play a particular role in intergranular sliding as their resistance to sliding is greater than other types of GBs. Thus, their spatial distribution and the different nature of GB intersections constitutes a useful piece of information to study grain boundary creep.

Displacement and strain field measurements at high temperatures by micro-extensometry

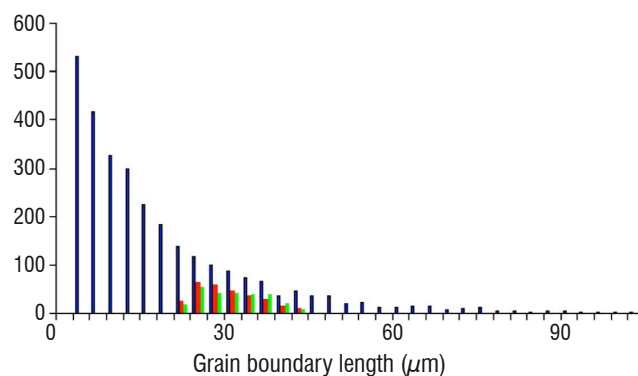
Micro-extensometry is a technique to measure local displacement and strains, well suited to study intergranular phenomena. In a SEM, it is based on image correlation techniques of the observed sample's polished surface before and after deformation. As previously discussed, if the surface does not contain natural markers that can be identified on the SEM image, then it is necessary to introduce artificial features on the surface, for instance by engraving [22][4], internal marking [2], or film deposition [18][20][24]. In the work done at ONERA, the contrast was achieved by depositing a surface grid by electronic micro-lithography. The SEM images of the surface produced in this way were obtained from before and after *ex-situ* creep tests. The processing is done by a suitable image correlation algorithm that is

capable of tracking the position of the micro-lithography markers, in order to calculate the displacement fields. From the latter, the strain fields and the amplitude of the GB slidings are extracted.

The creep specimen marking by electronic micro-lithography was performed within the SEM chamber and involved the deposition of a ≈ 10 nm thin film of a different material on the polished sample surface following a particular pattern. In this study, it consisted of a $0.3 \times 5 \mu\text{m}$ grid over a $320 \times 320 \mu\text{m}$ area. The different stages involved in the micro-lithography process are shown schematically in Figure 6. It is worth noting that the grid material is deposited by either evaporation or spraying and must satisfy several criteria. For instance, its atomic number must be significantly different from that of the sample material in order to provide a good contrast in the SEM images obtained by Back Scattered Electron (BSE) signals. In addition, the microgrids were exposed to temperatures of 700°C during the creep test. Even though creep tests were performed in a vacuum, there is always a small partial oxygen pressure that may compromise the microgrid stability. Thus, the latter is another important requirement for the micro-grid material. Finally, the microgrid must be capable of



(a)



(b)

Figure 5 – (a) Grain boundary network with boundaries of the $\Sigma 3$ type in red and generic ones in green, both of between 20 to 40 μm in length, and with the blue GBs being generic ones of other sizes, and (b) distribution of the GB lengths identified in (a)

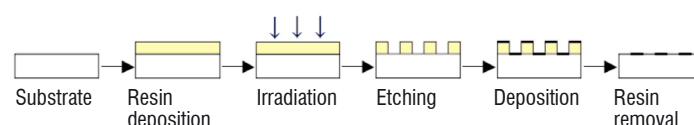


Figure 6 – Principal steps of the SEM micro-lithography deposition process

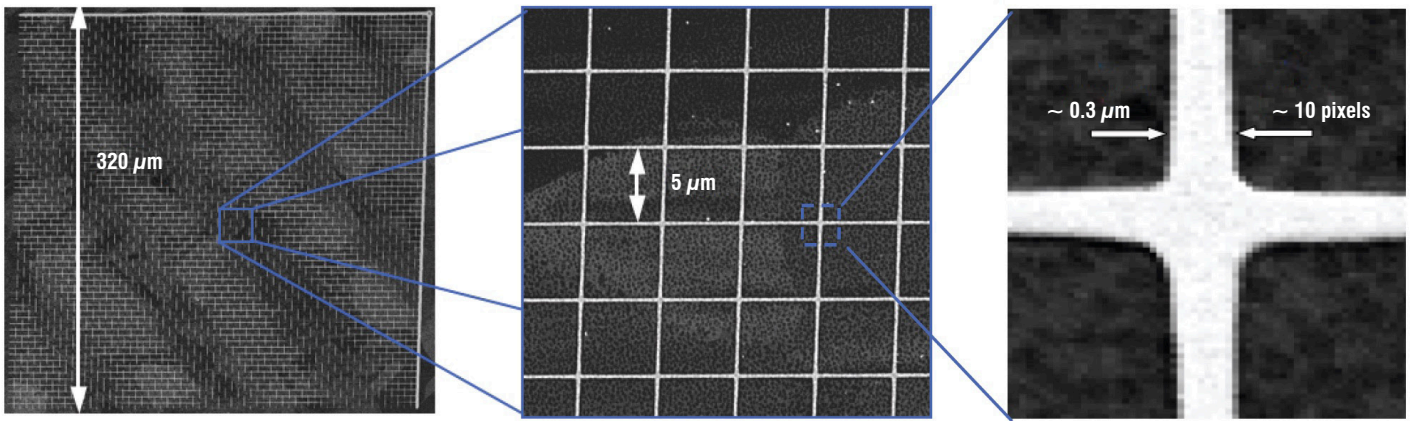


Figure 7 – SEM image of the microgrid produced by micro-lithography deposition in backscattered contrast

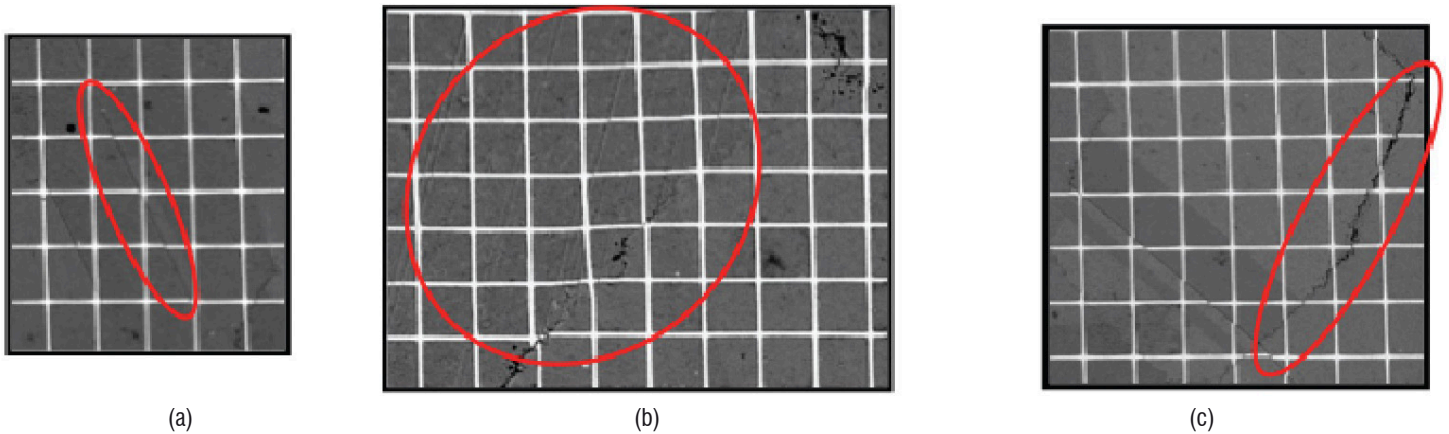


Figure 8 – Deformation phenomena revealed by the deformed microgrid: (a) intragranular shear, (b) localized plastic deformation or slip near a GB, and (c) intergranular shear

accommodating the substrate deformation without compromising its adhesion and mechanical integrity. Amongst the various options considered here, the material that best fulfilled the above requirements was HfO_2 , deposited as a thin film of ≈ 10 nm by cathodic spraying.

The image correlation (IC) method used to obtain the displacement and strain fields requires high resolution images with a good image-to-noise ratio. For that purpose, the electron beam current and acquisition time must be optimized. It should also be noted that, since the microgrid nodes constitute the markers that the IC will follow, they should be represented by a sufficient number of pixels. For instance, for the $0.3 \mu\text{m}$ wide microgrid lines shown in Figure 7, 7 to 8 pixels are typically required across the line width. Then, the pixel size that would be required in this case is approximately $0.04 \mu\text{m}$ in size. Other issues that condition the pixel size choice are the image size and acquisition time desired. For the $320 \times 320 \mu\text{m}$ image size shown in Figure 7, a minimum of 8000×8000 pixels will be required. The acquisition time for such an image size using the SEM system described here is of the order of 30 min.

The creep deformation of the superalloy at high temperatures reveals itself in different forms, through the microgrid deformation as well as the shearing and curvature of its originally straight segments. In Figure 8, it is possible to distinguish (a) intragranular shear, (b) localized plastic deformation or slip within the grain or near GBs, and (c) intergranular shear.

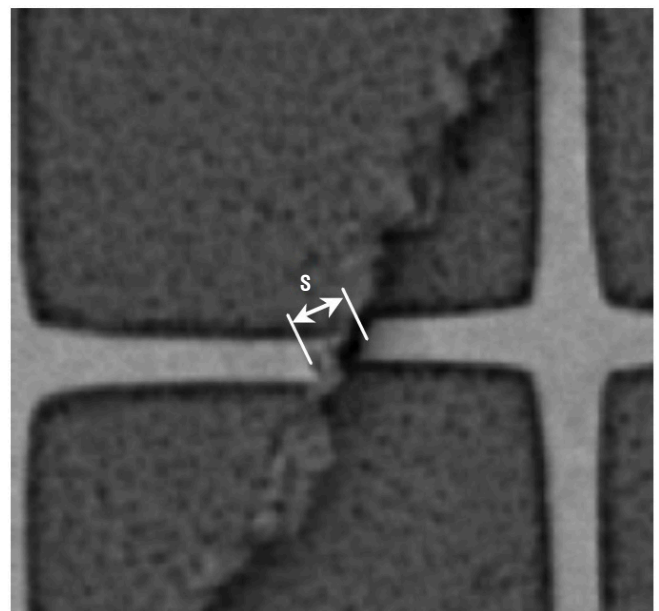


Figure 9 – Typical sheared grain boundary and attached microgrid with an associated shear displacement vector

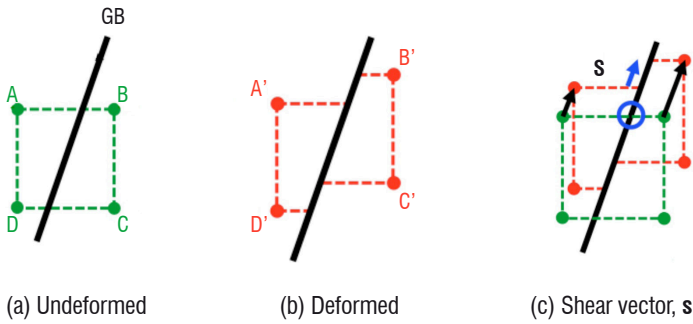


Figure 10 – Determination of the shear displacement vector at a GB-microgrid intersection

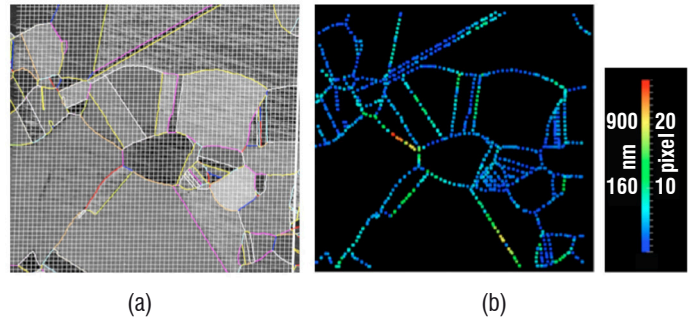


Figure 12 – (a) Superposition of the SEM and GB network images, and (b) corresponding plot of the GB shear displacement amplitudes

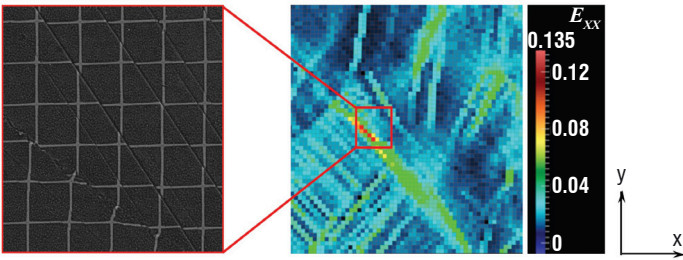


Figure 11 – Example of the local distribution of the E_{xx} strain component calculated from the microgrid after deformation. The zoomed image shows the deformed microgrid corresponding to the framed square in the right hand side image

The calculation of the strain associated with a sheared grain boundary is based on the displacement vector which characterizes the direction and amplitude of the localized shear deformation of the straight microgrid segment. This is given by the vector \mathbf{s} in the deformed microgrid shown in Figure 9. The determination of the shear displacement vector \mathbf{s} in the discrete microgrid node space relies on a comparison between the undeformed and deformed microgrids, as illustrated in Figure 10. It is then possible to represent the shear displacement amplitude across each microgrid-grain boundary intersection according to a color code associated with a reference scale.

Figure 11 shows a typical example of the local distribution of the strain component along the x -axis, calculated from the deformed microgrid. A part of the latter can be seen in Figure 11's zoomed region.

Combination of deformation and crystallographic data

The combination of the local crystallographic characteristics with the measured deformation fields contained in the EBSD and SEM images, respectively, require that they be available in the same reference system provided by the microgrid. However, this is not something that can be easily done as the operational conditions are quite different. For instance, in EBSD the sample is inclined at an angle of 70° with respect to the electron beam, whereas the latter is normal to the sample during the SEM imaging. It is also impossible to obtain both types of images of exactly the same physical region. Nevertheless, the most important difference is the size of the digital sampling; in this work, they were typically 2000×2000 pixels for the EBSD, and 8000×8000 pixels for the SEM images.

In order to make the EBSD and SEM images compatible, they need to be mapped into the same numerical space. The mapping of the

EBSD images into the resolution of the SEM images is done by a homography method based on the selection of point correspondences in the associated image pair. Here, four singular points that have corresponding ones in the two image domains are defined, and the subsequent superposition of the two images enables the validation of the procedure by data correlation. This can be seen in Figure 12(a), which shows an example of the superposition of the SEM and GB network images after the mapping procedure.

Once the mapping is done, the process of measuring the GB shearing can begin. It is convenient to assign a color code to the magnitudes of the GB shear displacements, in order to obtain quantitative plots of the microstructural region of interest. Figure 12(b) shows such a plot of GB shear displacement amplitudes for the image identified in Figure 12(a). In view of the fact that individual grains can now be identified by their own morphological and crystallographic characteristics, a range of additional information can be extracted. For instance, the mean shear amplitude of different types of grain boundaries, such as the proportion of $\Sigma 3$ and other generic type of GBs. An example is given in Figure 13, which shows the effect of the type of grain boundary and creep temperature on the GB mean shear displacements measured after creep tests at 350 MPa. The results reveal that the $\Sigma 3$ boundaries in Ni-base superalloys are more creep-resistant than those with greater coincidence indexes, with the GB shear displacement decreasing with temperature. One reason for such behavior is that recovery processes at high temperatures, such as that arising from dislocation annihilation, is much slower in CSL boundaries than in general boundaries due to the associated lower point defect diffusion kinetics. An additional mechanism reported by [30] is that dislocations accumulate at CSL boundaries, giving rise to internal stresses, which inhibits the dislocation motion.

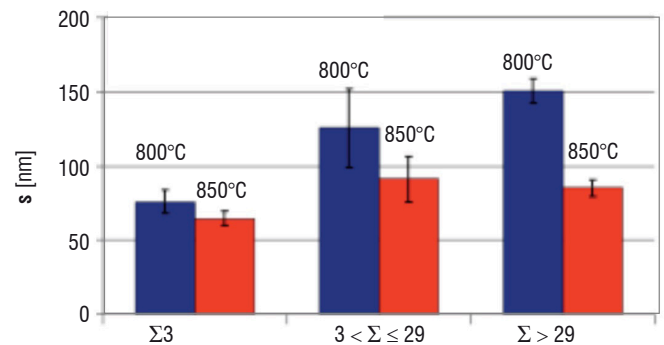


Figure 13 – Effect of the type of grain boundary and temperature on the GB mean shear displacement after a creep test at 350 MPa

Additional creep tests at 700°C and 800°C under an applied stress of 700 MPa were also carried out to investigate the effect of temperature on the deformation of the superalloy. Figures 14(a) and (b) show a comparison between the measured mean GB shear displacement vectors at these two temperatures. It can be seen that GB shear displacement decreases with temperature, from a maximum value of 113 nm at 700°C to 60 nm at 800°C. The contribution of GB sliding to the overall creep deformation along the loading direction was found to decrease from 33 % to 19 % for the same increase in temperature. This somehow counter-intuitive result is due to the known decrease of γ' -precipitate shearing activity by the γ -phase dislocations with temperature. Such shearing promotes deformation localization within narrow and planar slip bands, and leads to grain boundary shearing due to the high levels of stress concentration that develop at slip band- grain boundary intersections [27]. As temperature increases, the deformation becomes more homogeneous as matrix dislocations are now able to circumvent the precipitates through thermally activated mechanisms (e.g., climb, cross-slip), and the amplitude of grain boundary sliding decreases.

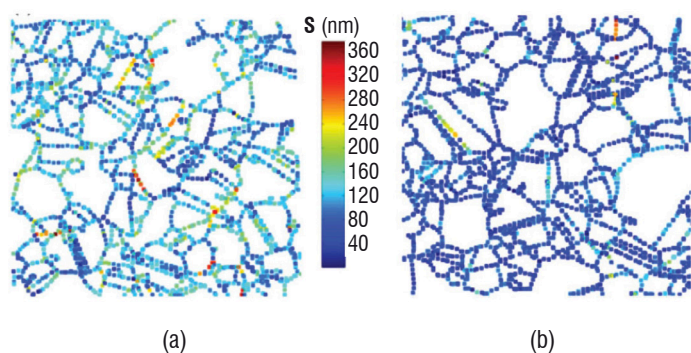


Figure 14 – Comparison between measured amplitudes of GB shearing displacements at two different temperatures: (a) 700°C and (b) 800°C

It is worth noting that superalloy microstructures can also exhibit very different GB morphologies depending on their metallurgical history. An interface or GB exhibiting a rather smooth morphology is likely to behave differently at high temperatures where GB sliding becomes an important deformation mechanism than one containing a rough or tortuous morphology. The results of an investigation of such GB morphology effects are presented in Figure 15, which shows a comparison between the measured amplitudes of GB shearing displacements in superalloy microstructures with the two different GB morphologies shown in the insets: (a) smooth and (b) tortuous. It can be seen that the inhibition of GB sliding due to the introduction of tortuous GBs leads to a significant decrease in the amplitude of the GB sliding. Such beneficial effect of GB morphology on the high-temperature behavior of superalloys is one of the GB engineering parameters being considered at ONERA for the next generation of polycrystalline superalloys.

In this section, the application of the combined SEM and EBSD techniques to study intergranular sliding in a Ni base superalloy under high temperature creep conditions has revealed the potential of such techniques to study and quantify complex deformation phenomena at the grain level. However, its development and setup require a great deal of experimental effort and know-how, be it in the marking of

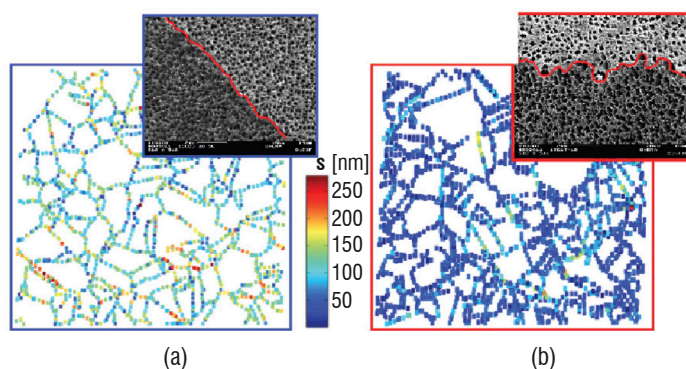


Figure 15 – Comparison between measured amplitudes of GB shearing displacements in superalloy microstructures with the two different GB morphologies shown in the insets: (a) smooth and (b) tortuous

samples by micro-electronic lithography, the data acquisition for the EBSD and SEM, or the development of the required software and post-processing tools.

Combined DIC with *in-situ* SEM and optical techniques to study multi-scale deformation phenomena

An illustration of how microstructural observation and mechanical characterization techniques can be combined inside the chamber of a SEM to study the deformation behavior of materials at two or more different microstructural scales is provided next. The need to simultaneously observe the evolution of the material microstructure at more than one scale can be found in a broad range of materials. A representative example is that of Nickel-base superalloys, widely used in aerospace and power generation applications, where microstructural heterogeneities can be found at different microstructural scales. As can be seen in Figure 16(a), mesoscale heterogeneities are introduced by the presence of 10-20 μm casting pores, usually found in the interdendritic regions, while those at the microscale (Figure 16(b)) result from the 0.5-1 μm γ' precipitates embedded in a nickel solid solution (γ) matrix. Typical micro-cracks which emanate from the casting pore, known to be due to localized deformation in the pore's vicinity (e.g., see [6]), can also be seen in Figure 16(a).

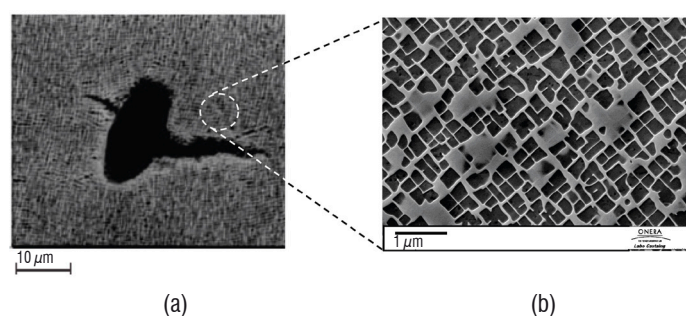


Figure 16 – Typical length scales associated with (a) a cracked casting defect [6] and (b) the superalloy $\gamma - \gamma'$ microstructure

Another class of materials that exhibits distinct observation scales are architected materials, where not only the intrinsic scales of the microstructure (e.g., the grain size) are relevant, but also that of its architecture arising from processing and/or manufacturing.

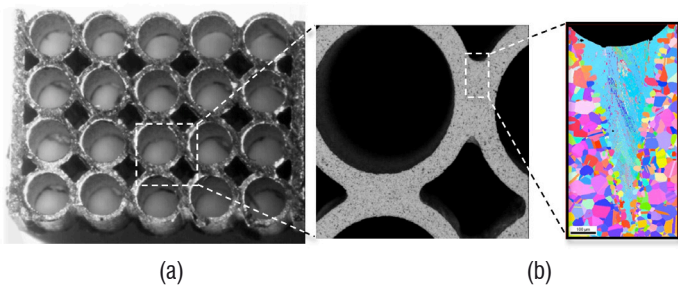


Figure 17 – Example of a multiscale architected material consisting of brazen Inconel tubes: (a) optical image at the scale of a group of tubes, and SEM images of (b) the local welded tubes and (c) the weld microstructure

A typical case is that of the multi-scale architected material shown in Figure 17, consisting of brazen Inconel tubes. Here, Figure 17(a) is an optical image at the scale of a group of tubes, and (b) and (c) are SEM images of the local brazen tubes and of the weld microstructure, respectively.

At ONERA, microscopists, metallurgists and engineers have recently developed a novel experimental *in situ* SEM setup to enable the simultaneous microstructural observation and measurement of the material deformation behavior at two different scales: a macroscopic one at the scale of the *in situ* specimen gauge length, and at the micrometer and nanometer scales associated with the actual material microstructure. By combining an *in situ* mechanical testing device, an optical microscope with a long lens and an SEM, it is possible to measure surface deformation fields over several millimeters and quantify the deformation at the scale of either individual grains in metals or fibers in composites. This original experimental set up, which has now been developed commercially and which has been named MEBIRIS, is illustrated in Figure 18. Here, the optical microscope

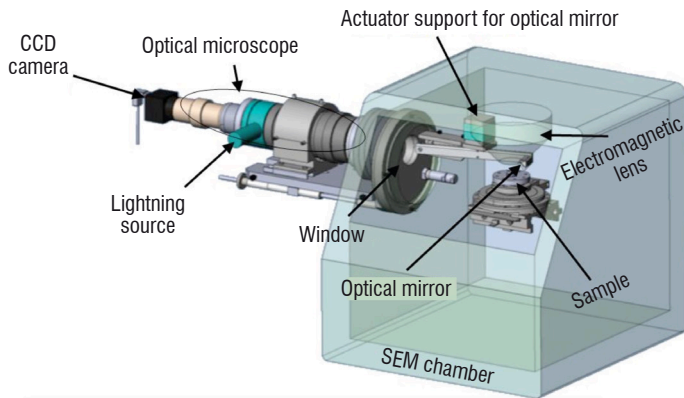


Figure 18 – Schematic set-up of the *in situ* SEM prototype named MEBIRIS

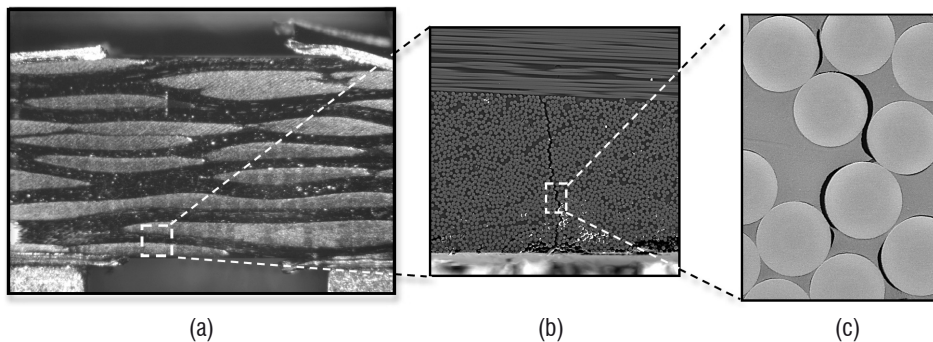


Figure 19 – Multiscale microstructure of a woven C fiber polymer matrix composite: (a) optical image at the scale of a strand of carbon fibers, and SEM images of (b) a crack inside an individual strand, and (c) of the decohesion between the fibers and the matrix

is externally mounted in one of the SEM ports. The resulting optical images are obtained with the help of a mirror positioned directly above the electronic beam column and inclined at an angle of 45° towards the microscope. The electronic image requires that the mirror be retractable. This was made possible by attaching it to an articulated arm driven by an externally controlled micro-motor.

For the development of MEBIRIS, it was necessary to respect a certain number of constraints, such as the optical performance defined by a variable field size (ranging from mm² to cm²), a focal plane capable of being positioned within a range of up to ~20 mm to follow a moving specimen (e.g., such as during a bending test), and the capability to obtain the acquired images with an error smaller than a pixel after the mirror retraction and insertion. There is also the need to precisely align the images obtained by optical means and by the SEM and for their centers to coincide. Additional challenges are associated with the fact that the SEM chamber works in a vacuum using a testing device mounted within the SEM chamber itself, and that an integrated lighting system is required for the optical microscope. Furthermore, no perturbations or noise can be tolerated by the SEM imaging.

An example of the capabilities of the prototype MEBIRIS will be shown next on a material with a multi-scale microstructure, namely the woven C-fiber polymer matrix composite shown in Figure 19. The main objective of this study was to simultaneously investigate during an *in-situ* tension test the development of mesoscopic cracks in the strand, and of interfacial micro-cracks resulting from the decohesion of the individual fibers from the matrix. For that purpose, optical and electronic images were captured alternatively during the test. Figure 19(a) shows an optical image at the scale of a group of strands of carbon fibers, and (b) and (c) are SEM images of a crack inside an individual strand, and of the decohesion between the fibers and the matrix, respectively. In this particular example, the scales of the fibers (10 μm) and the strands (500 μm) are only accessible via the SEM, but not the collection of strands shown in Figure 19(a), since the region of interest here is too large to be observed by SEM and needs instead to be obtained using the optical microscope.

The optical image shown in Figure 19(a) covers the sample width in the gauge length region, 7.4 × 7.4 mm in size, with a 5 μm resolution per pixel. The acquisition time per image was of ≈ 200 ms. Figure 19(b)'s electronic image, on the other hand, enabled the observation of local damage in a 450 × 450 μm region of an individual fiber strand with a resolution of 0.2 μm per pixel. However, the acquisition time per image was 64 s. Here, the stress applied at the moment when the images were taken was 240 MPa.

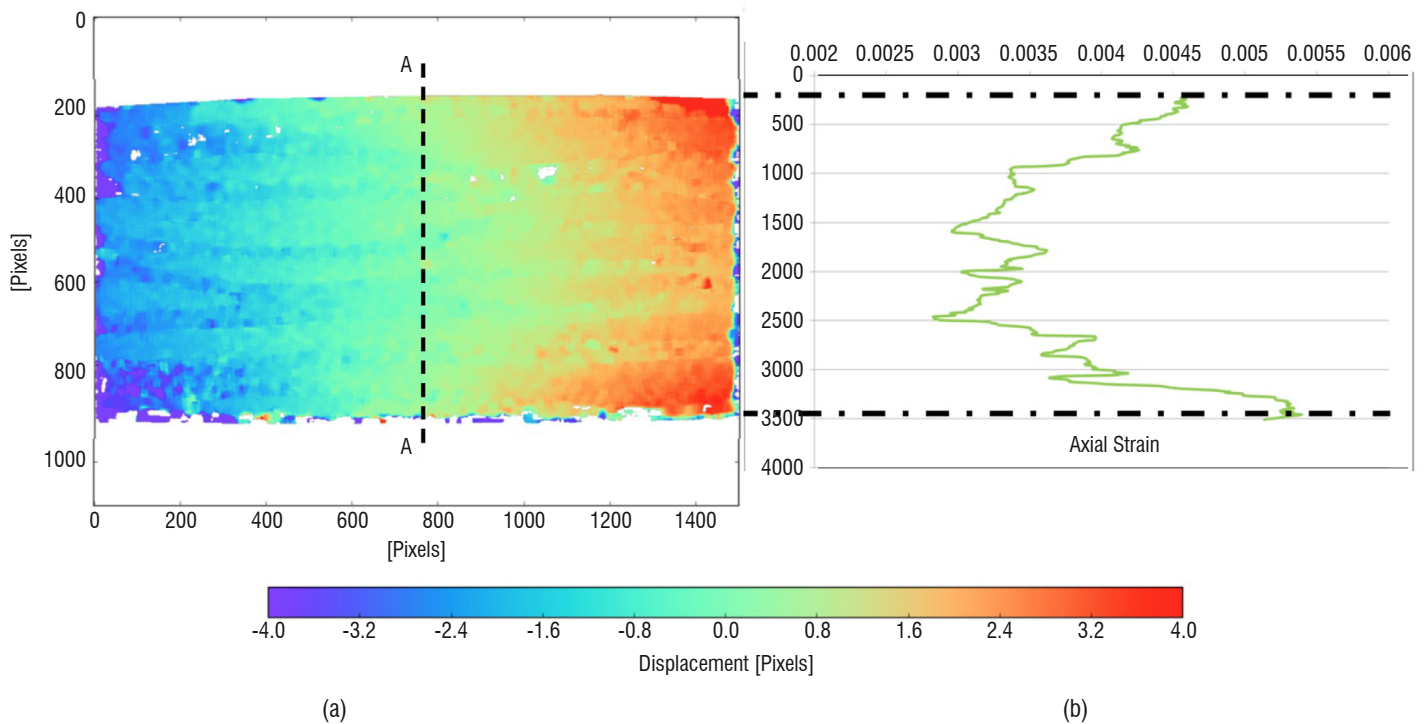


Figure 20 – (a) Measured axial displacements corresponding to Figure 19(a)'s optical image, and (b) axial strain profile along the line AA in (a) for an applied axial stress of 240 MPa

Figure 20(a) shows a color plot of the axial strains obtained by correlating the optical images such as that of Figure 19(a), between the undeformed and the deformed states, using the ONERA's FOLKI-D DIC method previously described. It can be seen that the quality of the optical images is sufficient for the image correlation. It is also possible to distinguish from the plot of the axial strain distribution the different deformation behavior exhibited by the axial and transverse strands. Figure 20(b) presents the measured axial strain profile across the composite specimen thickness, varying from 0.45 % at the surface, to about 0.30 % at its center. These values are consistent with those measured from macroscopic uniaxial tensile tests on the composite. From these type of measurements, a mean value of axial strain can be extracted for each of the loading steps to obtain an estimate of the average linear elastic stiffness of the composite. In this work, a value of $E = 77.3$ GPa was found, which compares well with the Young modulus of 72 ± 2 GPa measured macroscopically.

Concluding remarks

In this overview, we have discussed different techniques to describe local 2D and 3D material microstructures and to measure their deformation behavior. Several examples of *in-situ* or *ex-situ* morphological

and structural imaging of heterogeneous materials have been given. A comparative discussion between the classical global and local DIC approaches with the pixel-wise resolution ONERA approach, FOLKI-D, revealed considerable improvements of the latter in both resolution, due to its one-displacement vector-per-pixel architecture, and computational time arising from its suitability for parallel computing implementation using GPUs.

A contrast was provided between EBSD and optical and electron microscopy techniques, highlighting their complementarity. It is anticipated that the combination of different characterization and measurement techniques will significantly accelerate in the near future, to address outstanding issues related to multi-scale deformation phenomena spanning a few hundred of nanometers (defect) to a few micrometers (grain). This will likely involve the combination of techniques such as SEM, TEM, EBSD, EDS, tomography, DIC, thermography and improved software to integrate the resulting combined data sets for model calibration and validation. It is also expected that these advances will lead to the use of *in-situ* techniques combining experimental and numerical methods, including imaging over a broader range of length scales, and real-time computations to study the behavior of novel materials with complex heterogeneous microstructures ■

Acknowledgements

The authors are very grateful to Jean-Didier Garaud and Guy Le Besnerais from ONERA, for the discussions on the numerical aspects of the DIC work, and to A. Soula and K. Thibault for their doctoral research, which provided the foundations for some of the results of the case studies discussed here.

Bibliography

- [1] E. BAR-KOCHBA, J. TOYJANOVA, E. ANDREWS, K.-S. KIM, C. FRANCK - *A Fast Iterative Digital Volume Correlation Algorithm for Large Deformations*. Exp. Mechanics, V. 55(1), 2015, 261-274.
- [2] R.L. BELL, C. GRAEME-BARBER - *Surface and Interior Measurements of Grain Boundary Sliding During Creep*. Journal of Materials Science, 5, 1970, 933-944.
- [3] M. BORNERT, F. BREMAND, P. DOUMALIN, *et al.* - *Assessment of Digital Image Correlation Measurement Errors: Methodology and Results*. Exp. Mech 49, 2009, 353-370.
- [4] H. BRUNNER, N.J. GRANT - *Deformation Resulting from Grain Boundary Sliding*. Transactions of the Metallurgical Society of AIME, 215, 1959, 48-56.
- [5] J-Y BUFFIERE, E. MAIRE, J. ADRIEN, J-P MASSE, and E. BOLLER, *In Situ Experiments with X Ray Tomography: an Attractive Tool for Experimental Mechanics*. Exp. Mech. V. 50, 2010, 289-305.
- [6] S. DUMOULIN, E. P. BUSSO, N. P. O'DOWD - *A Multiscale Approach for Coupled Phenomena in FCC Materials at High Temperatures*. Philosophical Magazine, V. 83 (31-34), 2003, 3895-3916.
- [7] F. CHAMPAGNAT, A. PLYER, G. LE BESNERAIS, B. LECLAIRE, S. DAVOUST, and Y. LE SANT - *Fast and Accurate PIV Computation Using Highly Parallel Iterative Correlation Maximization*. Exp. Fluids 50, 2011, 1169-1182.
- [8] S. FELD-PAYET, V. CHIARUTTINI, J. BESSON and F. FEYEL - *A New Marching Ridge Algorithm for Crack Path Tracking in Regularized media*. Int. J; Solids and Struct., V. 71, 2015, 57-69.
- [9] B. GRANT, H. STONE, P. WITHERS, and M. PREUSS - *High Temperature Strain Field Measurement Using Digital Image Correlation*. J. Strain. Anal. Eng. 44, 2009, 263-271.
- [10] F. HILD and H. D. ESPINOSA - *Full Field Measurements and Identification in Solid Mechanics*. Procedia IUTAM , 4, 2012, 1-6.
- [11] F. HILD and S. ROUX - *Comparison of Local and Global Approaches to Digital Image Correlation*. Experimental Mechanics V. 52, 2012, 1503-1519.
- [12] J.T. HAMMER, T.J. LIUTKUS, J.D. SEIDT, A. GILAT - *Using Digital Image Correlation (DIC) in Dynamic Punch Tests*. Exp. Mechanics, V. 55(1), 2015, 201-210.
- [13] F. LAGATTU, F. BRIDIER, P. VILLECHAISE and J. BRILLAUD - *In-Plane Measurements on a Microscopic Scale by Coupling Digital Image Correlation and In Situ SEM Technique*. Materials Characterization, V 56, Issue 1, 2006, 10-18.
- [14] G. LE BESNERAIS and F. CHAMPAGNAT - *Dense Optical Flow by Iterative Local Window Registration*. proc. IEEE International Conference on Image Processing 2005, IEEE, Vol. 1, 1-137.
- [15] G. LE BESNERAIS, Y. LE SANT and D. L'EVÊQUE - *Fast and Dense 2D and 3D Displacement Field Estimation by a Highly Parallel Image Correlation Algorithm*. Strain, V. 52, 2016, 286-306.
- [16] B.D. LUCAS and T. KANADE - *An Iterative Image Registration Technique with an Application to Stereo Vision in*. IJCAI 81, 1981, 674-679.
- [17] H. POMMIER, E.P. BUSSO, T.F. MORGENEYER and A. PINEAU - *Intergranular Damage During Stress Relaxation in AISI 316L-Type Austenitic Stainless Steels: Effect of Carbon, Nitrogen and Phosphorus Contents*. Acta Mat. 103, 2016, 893-908.
- [18] J.D. PARKER, B. WILSHIRE - *A Surface Measurement Study of Grain Boundary Sliding During Creep of a Two Phase, Copper-Cobalt Alloy*. Materials Science and Engineering, 29, 1977, 219-225.
- [19] J.-C. PASSIEUX, F. BUGARIN, C. DAVID, J.-N. PÉRIÉ, L. ROBERT - *Multiscale Displacement Field Measurement Using Digital Image Correlation: Application to the Identification of Elastic Properties*. Exp. Mechanics, V. 55(1), 2015, 121-137.
- [20] R.C. POND, D.A. SMITH, P.W.J. SOUTHERDEN - *On the Role of Grain Boundary Dislocations in High Temperature Creep*. Philosophical Magazine, 37, 1978, 27-40.
- [21] L. PRIESTER - *Les joints de grains. De la théorie à l'ingénierie*. EDP Sciences, Les Ulis, 2000.
- [22] W.A. RACHINGER - *Relative Grain Translations in the Plastic Flow of Aluminium*. Journal of the Institute of Metals, 81, 1952, 33-41.
- [23] P. L. REU, W. SWEATT, T. MILLER, D. FLEMING - *Camera System Resolution and its Influence on Digital Image Correlation*. Exp. Mechanics, V. 55(1), 2015, 9-25.
- [24] C. REY, P. VIARIS DE LESEGNO, R. CHIRON - *Analysis of Shear Localization in Iron Crystals by Local Strain Field and Lattice Rotation Field Measurements*. Local Strain and Temperature Measurement, 1999, 30-39.
- [25] A. SOULA - *Étude de la déformation intergranulaire au cours du fluage à haute température d'un superalliage à base de nickel polycristallin*. Doctoral Thesis, INPG, Grenoble, 2008.
- [26] A. SOULA, Y. RENOLLET, D. BOIVIN, J.-L. POUCHOU, D. LOCQ, P. CARON, Y. BRECHET - *Analysis of High-Temperature Creep Deformation in a Polycrystalline Nickel-Base Superalloy*. Materials Science and Engineering A 06, 2009, 510:301-306.
- [27] A. SOULA, D. LOCQ, D. BOIVIN, Y. RENOLLET, P. CARON, Y. BRECHET - *Quantitative Evaluation of High Temperature Deformation Mechanisms: A Specific Microgrid Extensometry Technique Coupled with EBSD Analysis*. Journal of Materials Science 10, 2010, 45.
- [28] S.R. STOCK - *Recent Advances in X-Ray Microtomography Applied to Materials*. Int. Mater. Rev. 53(3), 2008, 129-181.
- [29] M. A. SUTTON, F. HILD - *Recent Advances and Perspectives in Digital Image Correlation*. Exp. Mechanics, V. 55(1), 2015, 1-8.
- [30] V. THAVEEPRIINGSRIPORN and G.S. WAS - *The Role of CSL Boundaries in Creep of Ni-16Cr-9Fe at 360°C*. Metall. Trans. 28A, 1997, 2101.
- [31] K. THIBAUT - *Influence de la microstructure sur le glissement intergranulaire lors du fluage d'un superalliage pour disques*. Doctoral Thesis, INPG, Grenoble, 2012.
- [32] K. THIBAUT, DIDIER LOCQ, PIERRE CARON, DENIS BOIVIN, YVES RENOLLET, YVES BRECHET - *Influence of Microstructure on Local Intra- and Intergranular Deformations During Creep of a Nickel-Based Superalloy At 700°C*. Mat. Sci. and Eng. A 12, 2013, 14-21.

AUTHORS



Esteban Busso is currently the Scientific Director of ONERA's Materials and Structures Division. He was formerly Professor of Mechanics of Materials at the *Ecole des Mines* de Paris and director of the *Ecole's Centre des Matériaux* and, from 1994 till 2005, Professor at Imperial College's Department of Mechanical Engineering in London, UK. He obtained his MSc and PhD degrees from the Massachusetts Institute of Technology (MIT) in Cambridge, USA, in 1987 and 1990, respectively. He also worked in industry in the UK, Japan, South Africa and Argentina. His research involves micromechanics studies of deformation and fracture of materials and interfaces, with an emphasis on the development of multiscale and multiphysics concepts in mechanistic models to predict deformation and fracture processes.



Denis Boivin is a senior research scientist with 30 years of experience in scanning electron microscopy with associated microanalysis and crystallographic EBSD techniques. He obtained his degree in instrumental physics from the *Conservatoire National des Arts et métiers* in Paris, France, in 1991. Taking advantage of the acquired experience along side high level specialists at ONERA, he now leads the Scanning Electron Microscopy laboratory, where improvements and control of the existing characterization techniques are continuously maintained to the benefit of materials research.



David Lévêque is a senior research scientist with 20 years of experience in mechanics of materials for aerospace applications. He obtained his PhD degree from the *Ecole Normale Supérieure* in Cachan, France, in 1998. Since his hiring at ONERA, he has been involved in several multi-partner national and international projects on composite and metallic materials (French-Japanese supersonic cooperation, CleanSky, ATLASII, ITP2, etc.). He now leads the Mechanical Characterization Laboratory, which is dedicated to the metallic material characterization and the development of various high temperature instrumented tests to better understand and identify the mechanical behavior of high temperature materials.